Received: 29 January 2026 | Revised: 20 May 2026 | Accepted: 26 June 2026 | Published online: 22 July 2026

RESEARCH ARTICLE

Journal of Optics and Photonics Research
2026, Vol. 00(00) 1–7
DOI: 10.47852/bonviewJOPR62029245

BON VIEW PUBLISHING

Study on Structural and Optical Properties of Nanocrystalline Mn–Ni Ferrites Prepared by Auto-Combustion Technique

Laxmi J. Hathiya[1,*] and Hiren H. Joshi[1]

[1] *Department of Physics, Saurashtra University, India*

Abstract: Nanocrystalline mixed ferrites with the general formula $Mn_xNi_{1-x}Fe_2O_4$ (x = 0.0 to 1.0, in steps of 0.2) were successfully synthesized using the auto-combustion technique. The main objective of this work was to investigate the effect of Mn substitution at Ni sites on the structural and optical properties of $NiFe_2O_4$ in the nanocrystalline regime. X-ray diffraction (XRD) reflections were consistent with the formation of a cubic spinel structure for all compositions. No additional crystalline impurity peaks were detected within the sensitivity of conventional powder XRD. The average crystallite size estimated from the Scherrer equation lies in the range of 26–33 nm, confirming the nanocrystalline nature of the synthesized powders. The slight variation in crystallite size with increasing Mn content suggests that ionic substitution influences the growth kinetics during combustion synthesis. Ultraviolet–visible (UV–Vis.) diffuse reflectance spectroscopy was used to study the optical response, and the apparent optical bandgap values were estimated from UV–Vis. absorbance data using Tauc analysis. The bandgap varies from 1.18 to 1.58 eV, revealing clear composition-dependent optical tuning. These results show that Mn substitution effectively changes the electronic structure and optical response, making $Mn_xNi_{1-x}Fe_2O_4$ ferrites favorable materials for optoelectronic and photocatalytic applications.

Keywords: nanoferrites, auto-combustion, XRD, UV–Vis., DRS

1. Introduction

Spinel ferrites with the common formula MFe_2O_4 (M = Mn, Ni, Co, Zn, etc.) represent an important class of magnetic oxide nanomaterials whose structural, magnetic, electrical, and optical properties can be modified by controlling cation distribution between tetrahedral (A) and octahedral [B] sites in the cubic spinel lattice [1–6]. Because of their chemical stability, tunable electronic structure, and moderate magnetization, spinel ferrites have attracted considerable interest for applications in photocatalysis, magnetic hyperthermia, microwave devices, spintronics, gas sensing, and environmental remediation [1, 7]. In photocatalytic systems in particular, spinel ferrites offer the combined advantages of visible-light response and magnetic recoverability, which make them attractive for pollutant degradation and water-treatment applications [7].

The optical and electronic behavior of spinel ferrites is governed by several interacting factors, including cation distribution, oxidation state, lattice distortion, and defect chemistry [7, 8]. The mixed valence states of iron, together with the flexible site occupancy of transition-metal cations, strongly influence charge-transfer transitions, crystal-field effects, and the density of localized states near the band edges [9, 10]. Through cation substitution, it is possible to modify the Fe–O–M bonding network, alter the degree of inversion, and tune the optical absorption characteristics over a wide range. For this reason, substituted ferrites are widely studied as compositionally tunable functional materials [2, 7].

Within this broader class, mixed Mn–Ni ferrite systems have emerged as particularly attractive because they combine the high magneto-crystalline anisotropy, chemical robustness, and relatively narrow bandgap with the variable valence (Mn^{2+}/Mn^{3+}) and strong lattice distortion effects associated with $MnFe_2O_4$ [2, 11, 12]. $NiFe_2O_4$ typically exhibits a partially inverse cation distribution with Ni^{2+} ions predominantly at octahedral sites, leading to significant anisotropy and moderate bandgap values suitable for visible-light activation [1, 8–10]. In contrast, $MnFe_2O_4$ tends toward more flexible cation arrangements and stronger Jahn–Teller distortions when Mn^{3+} is present, which can modify Fe–O–M super-exchange pathways and alter the density of states near the Fermi level [13]. Combining these two end members in $Mn_xNi_{1-x}Fe_2O_4$ thus provides a powerful compositional handle to engineer both magnetic and optical behavior through controlled Mn substitution at Ni sites [14]. Such substitution can influence crystallite growth, local strain, Fe–O bond environment, and band-edge structure.

Recent studies on Mn-doped $NiFe_2O_4$ have shown that increasing Mn content can modify crystallite size, lattice parameter, and optical absorption behavior. In some cases, Mn incorporation has been reported to shift the optical absorption edge toward lower energies, thereby improving visible-light utilization

***Corresponding author:** Laxmi J. Hathiya, Department of Physics, Saurashtra University, India. Email: laxmihathiya@sauuni.ac.in

[10, 11, 14–17]. For example, some authors reported that low-level Mn and Zn substitution in $NiFe_2O_4$ prepared by co-precipitation leads to bandgap energies around 1.95–1.98 eV, with high crystallinity and limited structural disorder, which is advantageous for optoelectronic applications [18]. $NiFe_2O_4$ has been reported to exhibit a bandgap near 1.53 eV, whereas $MnFe_2O_4$ nanoparticles have shown a narrow optical bandgap of approximately 1.4 eV [19, 20]. These observations support the interpretation that $Mn_xNi_{1-x}Fe_2O_4$ compositions can exhibit bandgaps in a similar low-energy semiconducting range, although the exact values remain sensitive to synthesis conditions and optical analysis methodology.

The synthesis technique plays a significant role in determining the microstructure, cation distribution, and hence the functional properties of spinel ferrites. Conventional ceramic methods typically require prolonged calcination or sintering at temperatures above 1000 °C, which often leads to grain coarsening, broad size distributions, and partial loss of compositional homogeneity, thereby limiting their suitability for nanoscale optical studies [2]. In contrast, wet-chemical techniques such as sol–gel, co-precipitation, hydrothermal, and combustion methods enable lower processing temperatures, finer particle sizes, and better control over stoichiometry and morphology [1–3]. Among these, the auto-combustion technique is especially attractive because it is rapid, cost-effective, and capable of producing nanocrystalline ferrites at comparatively low external temperatures through a self-sustained exothermic redox reaction between metal nitrates and organic fuel [21–23].

Auto-combustion synthesis has been successfully applied to a variety of spinel ferrite compositions, including Ni–Zn and Mn–Ni systems, yielding nanoparticles with crystallite sizes typically in the 15–80 nm range and single-phased cubic spinel structures studied by XRD analysis [1, 24, 25]. Structural refinement of $Ni_{1-x}Zn_xFe_2O_4$ prepared via sol–gel auto-combustion has shown that this method provides not only good phase purity but also reliable extraction of lattice constants, oxygen positional parameters, and cation radii at A and B sites, enabling quantitative assessment of cation distribution and its impact on magnetic and transport properties [22]. Similar observations have been made for Ni/Zn-based ferrites synthesized by related auto-combustion routes, where homogeneous nanoscale particles and narrow size distributions are routinely achieved, thereby facilitating reproducible optical and magnetic measurements [5]. Compared to high-temperature ceramic processing, auto-combustion thus offers a rapid, low-cost, and energy-efficient pathway to obtain well-crystallized, less agglomerated nanoparticles suitable for thin-film deposition and detailed optical characterization [3].

Despite the increasing number of literatures on Mn- and Ni-based ferrites, several important gaps remain. Many studies on Mn-doped $NiFe_2O_4$ focus on a limited number of compositions or narrow doping ranges and often employ synthesis methods such as simple co-precipitation or conventional ceramic processing that can complicate the interpretation of structure–property relationships due to significant variations in grain size, porosity, and defect density [11, 14]. In addition, individual reports frequently present XRD-derived lattice parameters or crystallite sizes and, separately, optical bandgap values from ultraviolet–visible (UV–Vis.) diffuse reflectance spectroscopy (DRS), and systematic attempts to directly correlate these structural parameters with composition-dependent bandgap evolution across the full $Mn_xNi_{1-x}Fe_2O_4$ series (x = 0.0–1.0) remain relatively insufficient. A rigorous correlation is particularly important in mixed systems like Mn–Ni ferrites, especially when there is a difference between the radius of ions between Mn^{2+} (≈0.80 Å) and Ni^{2+} (≈0.69 Å) and the possibility of Mn^{2+} formation can simultaneously influence lattice strain, super-exchange interactions, and band-edge positions.

In this regard, the present work aims to systematically elucidate composition-dependent optical bandgap tuning in citrate-gel auto-combustion–synthesized $Mn_xNi_{1-x}Fe_2O_4$ (x = 0.0–1.0, step: 0.2) nanoferrites by studying the structural parameters obtained from X-ray diffraction (XRD) and optical bandgaps derived from UV–Vis. DRS and Tauc plot analysis. By synthesizing a complete series of compositions under identical combustion conditions, followed by careful evaluation of crystallite size and lattice parameter evolution. The novelty of the work lies in providing a coherent structure–optics correlation for the entire Mn–Ni compositional range at the nanoscale, thereby offering insights into how Mn^{2+} substitution at Ni^{2+} sites can be used as a design strategy to tailor bandgaps in spinel ferrites for targeted photocatalytic and optoelectronic applications.

2. Experimental Details

2.1. Materials

In this study, the nanocrystalline spinel ferrite powder samples of $Mn_xNi_{1-x}Fe_2O_4$ with x = 0.0, 0.2, 0.4, 0.6, 0.8, and 1.0 were synthesized by the citrate-gel auto-combustion route, as shown in Figure 1, using the EMSURE® ACS, ISO Reag. Ph Eur. (99%) Grade chemicals, manganese nitrate $Mn(NO_3)_2{\cdot}4H_2O$, nickel nitrate $Ni(NO_3)_2{\cdot}6H_2O$, ferric nitrate $Fe(NO_3)_3{\cdot}9H_2O$, citric acid $C_6H_8O_7{\cdot}H_2O$, and ammonia solution NH_3 (25%), procured from Merck, Germany.

As displayed in Figure 1, to create a homogeneous solution, the nitrates were dissolved in 100 mL of double-distilled water while being continuously stirred magnetically at room temperature. Citric acid was added, followed by dropwise addition of ammonia solution to reach pH 7, preventing selective precipitation. The mixture was heated to 80–120 °C on a hot plate with stirring, evaporating water to yield a viscous gel (~1–2 h). This gel was further heated at 180–200 °C, igniting a self-generating flameless auto-combustion reaction within minutes, generating voluminous fluffy ash via exothermic redox between nitrates and citrate. The as-burnt precursor was ground using an agate mortar-pestle into fine powder and baked at 200 °C for 2–4 h in a furnace

Figure 1
Graphic presentation of synthesis method of Mn–Ni nanoferrites

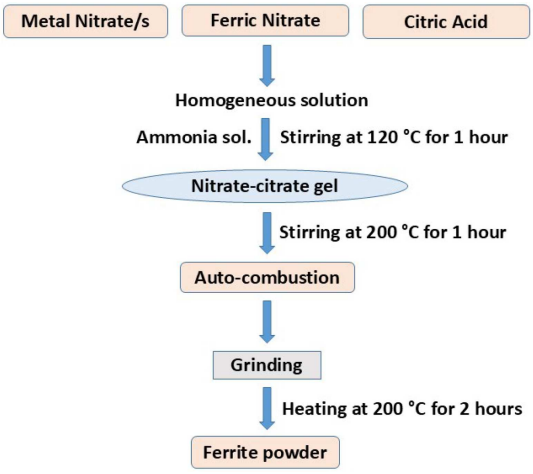

to remove impurities, enhance crystallinity, and obtain phase-pure nanostructured powders.

2.2. Characterizations

A Phillips X-ray diffractometer (PW 3040/60, X'pert PRO) was used in this study to measure XRD using Cu Kα radiation (λ = 1.5405Å) by continuously scanning in the range of 2θ from 20° to 80° at room temperature. The measurement of UV–Vis. DRS was conducted using a Shimadzu UV-1800 UV–Vis. spectrophotometer in absorbance mode, with a scanning range of 200–800 nm.

3. Results and Discussion

3.1. XRD

As shown in Figure 2, XRD was used at room temperature to examine the structure of synthesized nanocrystalline Mn–Ni ferrite powders.

The XRD patterns of all the samples were indexed by comparing the observed peak positions and relative intensities with the corresponding International Centre for Diffraction Data (ICDD) standard data for the cubic spinel structure relevant to the *Fd3m* space group. It was compared with the XRD patterns of pure $NiFe_2O_4$ and $MnFe_2O_4$ obtained from ICDD, as shown in Figure 3. The main reflections at (220), (311), (222), (400), (422), (333), and (533) match well with the standard spinel pattern, confirming the creation of a single-phase cubic spinel structure within the detection limit of XRD. The slight difference in intensity and broadening of the peak in the samples may be ascribed to changes in crystallite size, local strain, and cation distribution.

Figure 2
X-ray diffractograms of Mn–Ni ferrites

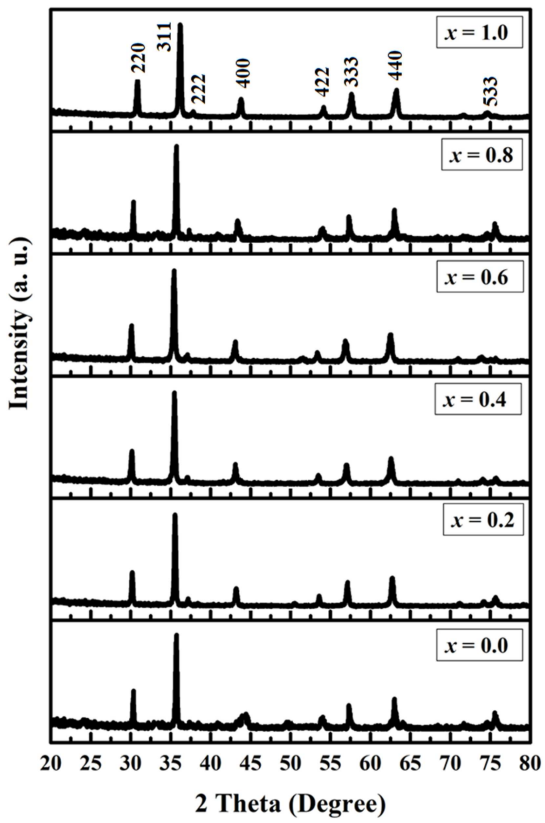

Figure 3
XRD patterns of (a) $NiFe_2O_4$ and (b) $MnFe_2O_4$ obtained from ICDD

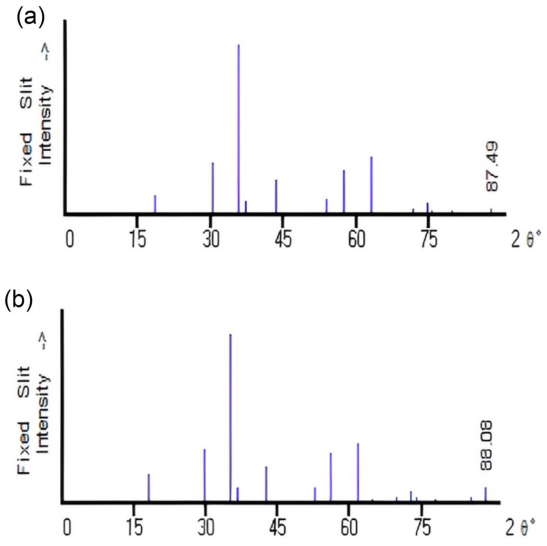

No additional peaks attributable to major impurity phases were observed, although the presence of minor secondary phases below the detection of XRD cannot be completely excluded.

The broad width of the diffraction peaks suggests the nanoscale characteristics of the final products [26]. The prominence of the (311) reflection at approximately 2θ = 35.5° confirms the formation of the spinel ferrite phase throughout the entire compositional range. The average crystallite size for all the nanocrystalline $Mn_xNi_{1-x}Fe_2O_4$ powder samples was calculated using the full width at half maximum (FWHM) of the strongest peak (311) by employing Scherrer's equation [27]:

$$D_{XRD} = \frac{k\lambda}{\beta cos\theta} \quad (1)$$

where k is a constant approximately equal to 0.9, λ is the wavelength (1.5405Å), θ is the Bragg's angle, and β is the FWHM in the radian. The calculated crystallite size for all the samples is shown in Table 1.

The increase in lattice parameters (Table 1) with an increase of Mn content in each synthesized sample can be attributed to the replacement of the cation with a smaller radius of ions Ni^{2+} (0.69 Å) by the larger one Mn^{2+} (0.80 Å). The substitution of Ni^{2+} ions with Mn^{2+} ions leads to an expansion in the interatomic distance, resulting in an increase in the lattice constant

Table 1
Lattice parameter and crystallite size of nanostructured $Mn_xNi_{1-x}Fe_2O_4$

Value of x	Lattice parameter a (nm) ± 0.0002	Crystallite size D_{XRD} (nm) ± 2
0.0	0.8340	33.80
0.2	0.8381	33.00
0.4	0.8390	28.28
0.6	0.8400	27.17
0.8	0.8409	25.20
1.0	0.8416	26.65

[28–31]. As shown in Table 1, notably, D_{XRD} exhibits a systematic decrease from $x = 0.0$ to $x = 0.8$, followed by a slight increase at $x = 1.0$ (pure $MnFe_2O_4$) from $x = 0.8$. This trend reflects the influence of Mn^{2+} incorporation, which has a larger ionic radius compared to Ni^{2+} ions. Progressive substitution induces lattice strain and modifies nucleation/growth kinetics during the rapid auto-combustion process, resulting in smaller coherent domains. The minimum size at $x = 0.8$ suggests optimal strain accommodation before phase stabilization effects dominate at the $MnFe_2O_4$ endpoint.

A further detail of the XRD patterns is the non-monotonic intensity variation at higher-angle reflections around $2\theta \approx 75°$. Such behavior may arise from subtle changes in local ordering, preferred orientation, or composition-dependent distribution of cations within the spinel framework. These intensity variations can be treated only as qualitative indications of evolving local structure rather than direct evidence of a specific cation arrangement.

3.2. UV–Vis. DRS analysis

To determine the optical bandgap of the synthesized Mn–Ni nanoferrites, UV–Vis. spectra were obtained in absorption mode within the range of 200–800 nm.

The optical bandgap of the synthesized $Mn_xNi_{1-x}Fe_2O_4$ spinel ferrite powder samples was determined using the Tauc plot based on the UV–Vis. absorbance data illustrated in Figure 4. The bandgap of these nanoferrites is determined by assuming a direct transition between the valence band edges and conduction band through the following expression [32]:

$$(\alpha h\nu)^n = K(h\nu - Eg) \quad (2)$$

Figure 4
UV–Vis. absorbance spectra and Tauc plot of nanocrystalline $MnxNi_1$-xFe_2O_4 ferrite powders

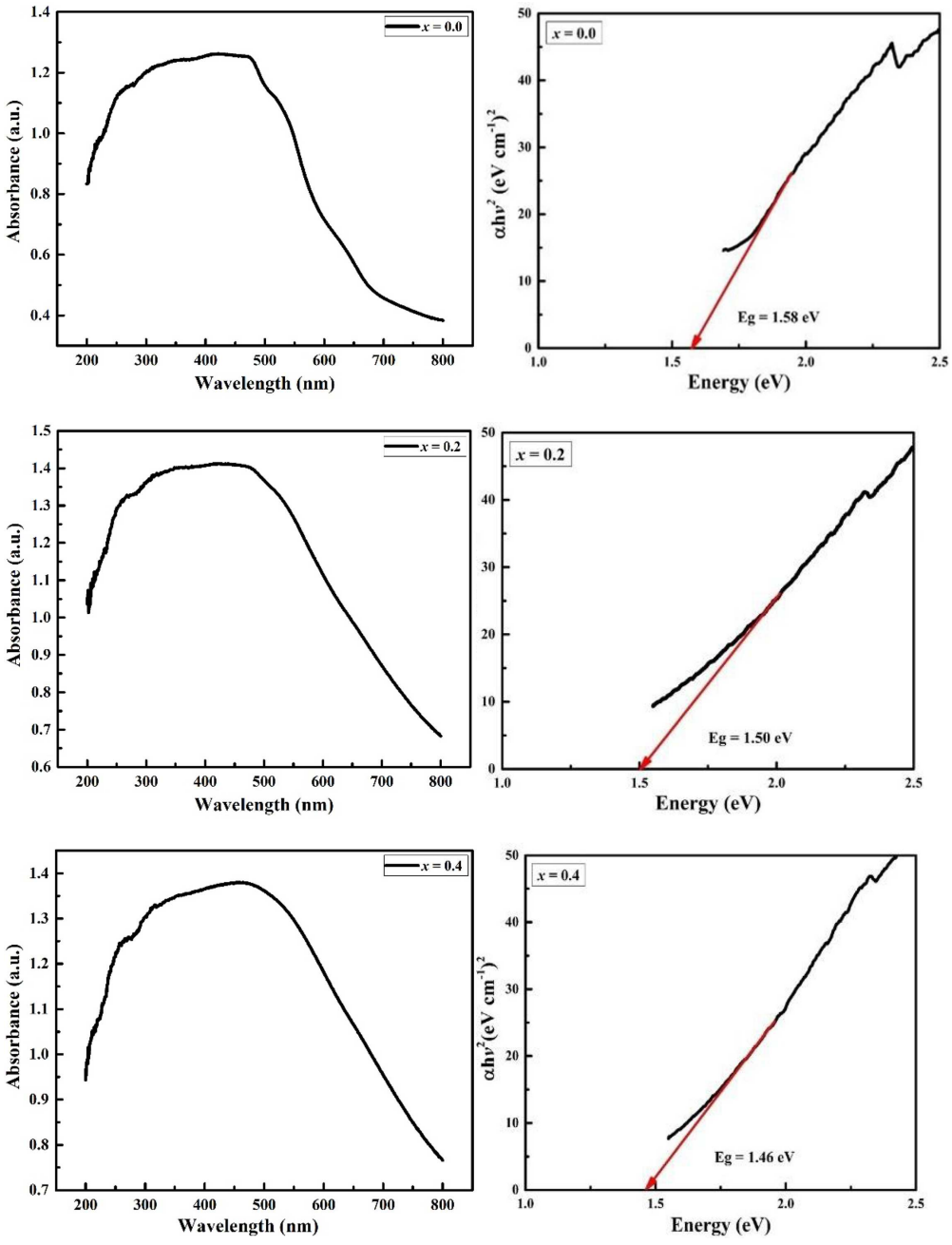

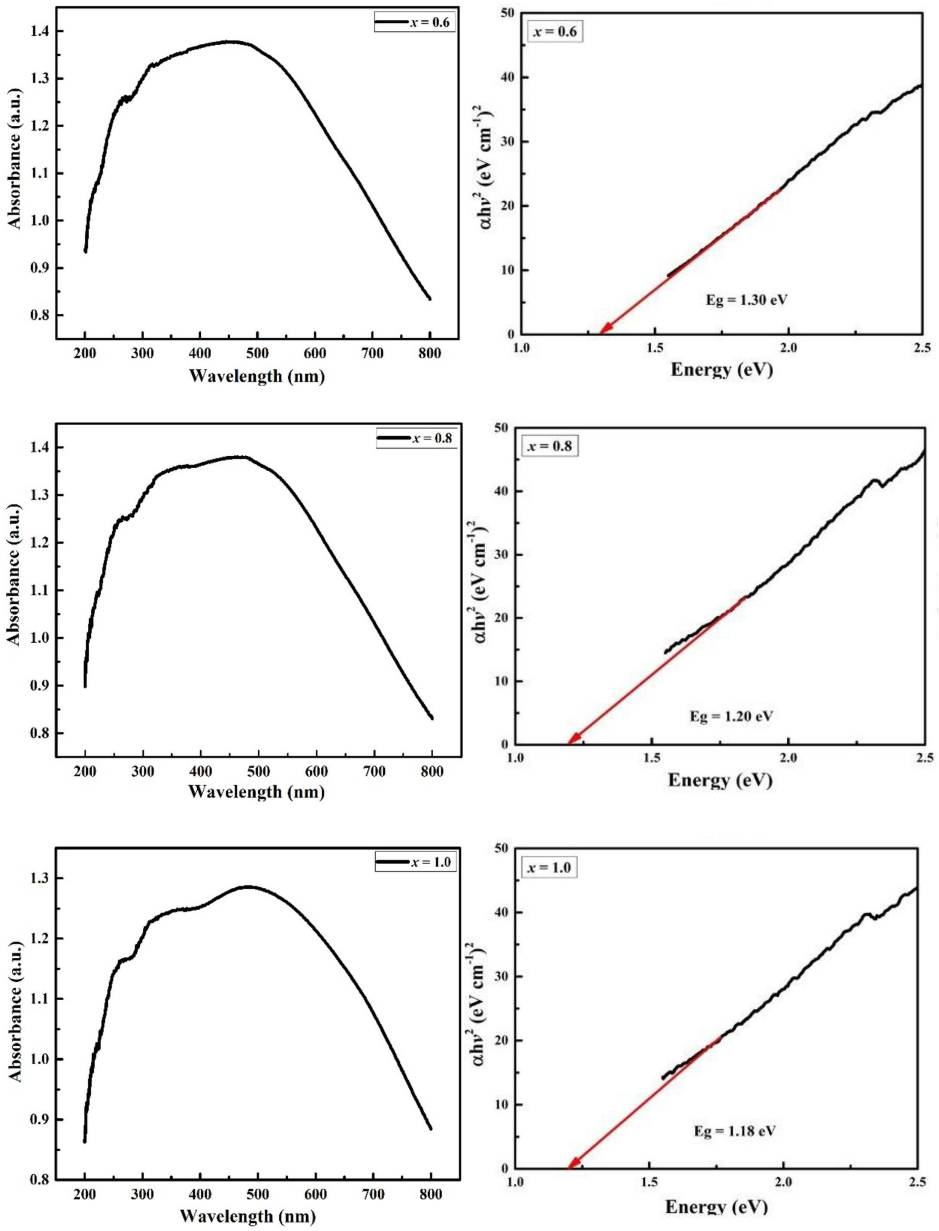

where α represents the absorption coefficient, hν signifies the energy of the incident photon, K denotes the energy-independent constant, Eg refers to the energy of the optical bandgap, and n is a constant that depends on the transition type, taking a value of 2 for a direct optical bandgap, while 1/2 for an indirect optical bandgap.

The values of the bandgap of all the samples are from 1.18 to 1.58 eV ($\pm$0.05 to $\pm$0.10), as depicted in Figure 4. These values are in accordance with the semiconducting range and are broadly consistent with many reports on nanoscale ferrites, although they differ from some published values for apparently similar Mn–Ni ferrite systems. Such discrepancies in the literature may arise from differences in spectral transformation, the use of raw absorbance instead of properly treated diffuse reflectance data, variation in Tauc fitting range, or differing assumptions regarding the transition type. As shown in the Tauc plots of the present ferrite system, the energy bandgap value of the synthesized $Mn_xNi_{1-x}Fe_2O_4$ nanostructured powders decreases with the increase of manganese ion content in every step of x, indicating the effect of substituents in the change of the structure of the basic lattice with increased lattice strain and altered cation inversion, as evidenced by systematic XRD peak broadening [33].

The observed shift in Eg with increasing Mn content correlates directly with the XRD-derived crystallite size reduction and lattice expansion. Several mechanisms contribute to this phenomenon: (i) Mn^{2+} ($3d^5$) introduces additional d-electrons that create impurity bands or donor levels near the conduction band minimum, narrowing the effective gap; (ii) larger Mn^{2+} ions increase the lattice constant, reducing Fe–O bond covalency and altering crystal-field splitting; and (iii) compositional tuning of cation inversion between A-site (tetrahedral) and B-site (octahedral) modifies Fe^{3+}–O^{2-} charge-transfer transitions, which dominate the valence-to-conduction band excitation [34]. In nanocrystalline ferrites, crystallite size reduction is also often accompanied by increased strain and defect concentration, which may contribute to the apparent narrowing of the optical bandgap. Therefore, the present results are interpreted as evidence of a composition-dependent structural-electronic response rather than as proof of a single dominant mechanism.

The direct correlation between decreasing crystallite size and narrowing bandgap further highlights the synergy between synthesis control and functional property optimization in auto-combustion-derived nanomaterials. This composition-tunable bandgap (1.18–1.58 eV) indicates the potential for applications in visible-light photocatalysis, photoelectrochemical cells, and energy-efficient optoelectronic devices.

4. Conclusion

The nanocrystalline ferrite powders of Mn^{2+}-substituted nickel ferrites were successfully prepared by the auto-combustion method to investigate their structural and optical properties. The crystal structure, phase formation, and crystallite size of the final products were determined by XRD measurement. The optical properties and energy bandgap values determined by UV–Vis. DRS analysis of the samples are within the values of semiconductors that confirm the synthesized Mn–Ni ferrites possess potential optical properties and can be used in semiconductors. These findings demonstrate effective structure–optics engineering in Mn–Ni ferrites for energy and environmental technologies.

Acknowledgement

The authors are thankful to Saurashtra University for the research facilities. The author (Laxmi J. Hathiya) is grateful to the University Grants Commission, New Delhi, for providing a research fellowship.

Ethical Statement

This study does not contain any studies with human or animal subjects performed by any of the authors.

Conflicts of Interest

The authors declare that they have no conflicts of interest to this work.

Data Availability Statement

Data sharing is not applicable to this article as no new data were created or analyzed in this study.

Author Contribution Statement

Laxmi J. Hathiya: Conceptualization, Methodology, Software, Formal analysis, Investigation, Data curation, Writing – original draft, Visualization. **Hiren H. Joshi:** Validation, Resources, Writing – review & editing, Supervision, Project administration.

References

[1] Salih, S. J., & Mahmood, W. M. (2023). Review on magnetic spinel ferrite (MFe_2O_4) nanoparticles: From synthesis to application. *Heliyon*, *9*(6), e16601. https://doi.org/10.1016/j.heliyon.2023.e16601

[2] Mataev, M., Madiyarova, A., Abdraimova, M., Tursyn, Z., & Ramachandran, K. (2026). Structure property–application relationships of spinel ferrite nanoparticles: From synthesis to functional systems. *International Journal of Molecular Sciences*, *27*(5), 2096. https://doi.org/10.3390/ijms27052096

[3] Sutka, A., & Mezinskis, G. (2012). Sol–gel auto-combustion synthesis of spinel-type ferrite nanomaterials. *Frontiers of Materials Science*, *6*(2), 128–141. https://doi.org/10.1007/s11706-012-0167-3

[4] Noreen, S., & Hussain, A. (2023). Structural, optical, morphological and magnetic properties of $Cu_{0.25}M_{0.75}Fe_2O_4$ (M = Mn, Mg, Ni and Co) ferrites for optoelectronic applications. *Optical Materials*, *139*, 113797. https://doi.org/10.1016/j.optmat.2023.113797

[5] Hossain, M. A., Rouf, H. K., Hossain, M., Alam, M. K., & Khan, M. N. I. (2025). Synthesis and exploration of structural, optical, magnetic, and electrical properties of Ti-doped Mn-Ni-Zn ferrite. *AIP Advances*, *15*(5), 055016. https://doi.org/10.1063/5.0265876

[6] Hathiya, L. J., Baraliya, J. D., Das, A., Sen, D., Gismelseed, A. M., Yousif, A. A., & Joshi, H. H. (2022). Anomalous magnetic behaviour at nano-scale of Mn^{2+}-substituted magnesio-ferrite synthesized by auto-combustion technique. *Indian Journal of Physics*, *96*(8), 2323–2335. https://doi.org/10.1007/s12648-021-02169-z

[7] Hall, C. A., Ferrer, P., Grinter, D. C., Kumar, S., da, Silva I., Rubio-Zuazo, J., ..., & Grau-Crespo, R. (2024). Spinel ferrites MFe_2O_4 (M = Co, Cu, Zn) for photocatalysis: Theoretical and experimental insights. *Journal of Materials Chemistry A*, *12*(43), 29645–29656. https://doi.org/10.1039/D4TA04941A

[8] Bajorek, A., Berger, C., Dulski, M., Zubko, M., Lewińska, S., Prusik, K., . . . , & Randrianantoandro, N. (2022). Tuning physical properties of $NiFe_2O_4$ and $NiFe_2O_4$@SiO_2 nanoferrites by thermal treatment. *Metallurgical and Materials Transactions A*, 1208–1230. https://doi.org/10.1007/s11661-021-06567-0 *53*(4)

[9] Patra, J., Parida, P., Singh, V. R., Patel, P., Sahoo, S. K., Mahapatra, S., . . . , & Verma, V. K. (2025). Effect of substrate temperatures on tunable band gap and optical properties of $NiFe_2O_4$ thin films. *Physica B: Condensed Matter*, *715*, 417610. https://doi.org/10.1016/j.physb.2025.417610

[10] Darul, J., & Piszora, P. (2023). Influence of lattice defects on the high pressure properties of $Ni_{0.66}Mn_{2.34}O_4$ NTC ceramics. *Ceramics International*, *49*(6), 9412–9418. https://doi.org/10.1016/j.ceramint.2022.11.106

[11] Asha, Juglan., C, K., & Jain, A. (2024). A review on magnetic properties, synthesis, characterization, and applications of Mn–$NiFe_2O_4$ ferrites. *AIP Conference Proceedings*, *2986*(1), 030127. https://doi.org/10.1063/5.0192528

[12] Hathiya, L. J., Rathore, D., & Joshi, H. H. (2025). Gas sensing application of nanomaterials. In M. F. Desimone, R. B. Jotania, R. B. Khomane, & R. G. Chaudhary (Eds.), *Nanotechnology: Applications for environmental protection and sustainability* (pp. 167–185). Springer. https://doi.org/10.1007/978-3-031-86508-4_8

[13] El-Masry, M. M., & Arman, M. M. (2025). Cobalt, nickel and zinc spinel ferrites with high transmittance and UV-blocking for advanced optical applications. *Scientific Reports*, *15*(1), 16636. https://doi.org/10.1038/s41598-025-99604-6

[14] Sarita, Anchal., Choudhary, S. R., Choudhary, Y., Bhamu, P. K., Pandey, J., . . . , & Choudhary, B. L. (2026). Multifaceted characterization of Mn-Doped nanocrystalline $NiFe_2O_4$ ferrites. *Journal of the Korean Physical Society*, *88*(4), 449–469. https://doi.org/10.1007/s40042-025-01514-3

[15] Oviya, K. J., & Sivagurunathan, P. (2024). Structural, magnetic and electrochemical properties of nickel manganese ferrite ($Ni_xMn_{1-x}Fe_2O_4$) nanoparticles prepared via

coprecipitation method. *Asian Journal of Chemistry*, *36*(10), 2375–2384. https://doi.org/10.14233/ajchem.2024.32404

[16] Gumma, A., Ugendar, K., Soumya, S., Durga Rao, T., Raghvendra Reddy, V., & Sattibabu, B. (2025). Impact of alkaline earth metal ion substitution on the structural and temperature-dependent magnetic properties of $NiFe_2O_4$ nanoparticles. *Ceramics International*, *51*(3), 3243–3253. https://doi.org/10.1016/j.ceramint.2024.11.303

[17] Al-Hunaiti, A., Ghazzy, A., Sweidan, N., Mohaidat, Q., Bsoul, I., Mahmood, S., & Hussein, T. (2021). Nano-magnetic $NiFe_2O_4$ and its photocatalytic oxidation of vanillyl alcohol—Synthesis, characterization, and application in the valorization of lignin. *Nanomaterials*, *11*(4), 1010. https://doi.org/10.3390/nano11041010

[18] Nazari, N., Golzan, M. M., & Mabhouti, K. (2024). Study of Urbach energy and Kramers–Kronig on Mn and Zn doped $NiFe_2O_4$ ferrite nanopowder for the determination of structural and optical characteristics. *Scientific Reports*, *14*(1), 6407. https://doi.org/10.1038/s41598-024-57045-7

[19] Pereira, M. S., Vasconcelos, V. M. R., Palácio, M. P. S., Oliveira, F. G. S., Santos, L. P. M., Vasconcelos, D. L. M., . . . , & Vasconcelos, I. F. (2021). Characterization of $CoFe_2O_4$, $NiFe_2O_4$, and $ZnFe_2O_4$ nanoparticles synthesized by a proteic sol-gel method. *Journal of Superconductivity and Novel Magnetism*, *34*, 2845–2853. https://doi.org/10.1007/s10948-021-05968-x

[20] Gurumoorthy, M., Palani, G., Trilaksanna, H., & Kumar, M. (2024). The structural, morphological, optical, thermal and magnetic properties of $MnFe_2O_4$ nanoparticles. *Analytical Chemistry Letters*, *14*(6), 848–861. https://doi.org/10.1080/22297928.2024.2420883

[21] Hasan, S., & Azhdar, B. (2022). Synthesis of nickel–zinc ferrite nanoparticles by the sol–gel auto-combustion method: Study of crystal structural, cation distribution, and magnetic properties. *Advances in Condensed Matter Physics*, *2022*(1), 4603855. https://doi.org/10.1155/2022/4603855

[22] Rabie, M., Abdelhamid, M., El Sawy, E., & Moustafa, M. (2026). Structure–property relationships in $Co_{0.5}Zn_{0.5}Fe_2O_4$ nanoparticles synthesized by sol–gel auto-combustion. *Journal of Alloys and Compounds*, 186539. https://doi.org/10.1016/j.jallcom.2026.186539 *1056*

[23] Rao, P. N., Boda, N., Nagendar, V., Chittury, K. L., Nithya, R., & Raju, A. (2026). Structural and DC electrical properties of samarium-substituted cobalt nanoferrites synthesized by citrate-gel auto-combustion method. *Journal of Sol-Gel Science and Technology*, *118*(3), 70. https://doi.org/10.1007/s10971-026-07177-1

[24] Kore, E. K., Kore, A. E., Shaikh, S. A., Nargundkar, G. P., Bandgar, S. S., Tamboli, S. L., . . . , & Chanmal, C. V. (2026). Magneto-structural correlation in $MnFe_2O_4$ nanocrystals synthesized by auto-combustion method. *Applied Physics A*, *132*(4), 290. https://doi.org/10.1007/s00339-026-09392-7

[25] Celik, C., Yasar, M., Alzahrani, K. J., Ashirova, A., Jadeja, Y., Roopashree, R., . . . , & Alsharif, K. F. (2026). Enhanced photocatalytic degradation of organic pollutants using cu-doped spinel ferrites synthesized via sol-gel auto-combustion: A study of structural, optical, and catalytic properties. *Journal of Sol-Gel Science and Technology*, *118*(1), 23. https://doi.org/10.1007/s10971-025-07031-w

[26] Priyadharshini, P., Pushpanathan, K., & Kathiravan, V. (2022). Effect of surfactants on the structural and magnetic properties of $NiFe_2O_4$ nanoparticles. *Asian Journal of Chemistry*, *34*(9), 2406–2414. https://doi.org/10.14233/ajchem.2022.23909

[27] Culity, B. D. (1956). *Elements of X-ray diffraction*. USA: Addison-Wesley.

[28] Hathiya, L. J., Rathore, D., Khan, M., & Joshi, H. H. (2024). Structural study and gas sensing application of nanocrystalline mixed ferrites synthesized by Auto-combustion method. *Journal of Materials Science: Materials in Electronics*, *35*, 1810. https://doi.org/10.1007/s10854-024-13586-1

[29] Phalake, S. S., Lad, M. S., Kadam, K. V., Tofail, S. A. M., Thorat, N. D., & Khot, V. M. (2022). Application of $Mn_xFe_{1-x}Fe_2O_4$ (x = 0–1) nanoparticles in magnetic fluid hyperthermia: Correlation with cation distribution and magnetostructural Properties. *ACS Omega*, *7*(48), 44187–44198. https://doi.org/10.1021/acsomega.2c05651

[30] Soudani, I., Mustapha, N., & Hjiri, M. (2026). Effect of divalent cation substitution (M = Mn, Ni, Mg, Cu) on the structural, magnetic and electrical properties of MFe_2O_4 spinel ferrites. *RSC Advances*, *16*(28), 25515–25528. https://doi.org/10.1039/D6RA02603F

[31] Dippong, T., Levei, E. A., Deac, I. G., Petean, I., & Cadar, O. (2022). Dependence of structural, morphological and magnetic properties of manganese ferrite on Ni-Mn substitution. *International Journal of Molecular Sciences*, *23*(6), 3097. https://doi.org/10.3390/ijms23063097

[32] Devi, G. S., Hyodo, T., Shimizu, Y., & Egashira, M. (2002). Synthesis of mesoporous TiO_2-based powders and their gas-sensing properties. *Sensors and Actuators B: Chemical*, *87*(1), 122–129. https://doi.org/10.1016/S0925-4005(02)00228-9

[33] Harish, K. N., Bhojya Naik, H. S., Prashanth Kumar, P. N., & Viswanath, R. (2013). Optical and photocatalytic properties of solar light active Nd-substituted Ni ferrite catalysts for environmental protection. *ACS Sustainable Chemistry & Engineering*, *1*(9), 1143–1153. https://doi.org/10.1021/sc400060z

[34] Mansour, S. F., Wageh, S., Al-Wafi, R., & Abdo, M. A. (2021). Enhanced magnetic, dielectric properties and photocatalytic activity of doped Mg–Zn ferrite nanoparticles by virtue of Sm^{3+} role. *Journal of Alloys and Compounds*, *856*, 157437. https://doi.org/10.1016/j.jallcom.2020.157437

How to Cite: Hathiya, L. J., & Joshi, H. H. (2026). Study on Structural and Optical Properties of Nanocrystalline Mn–Ni Ferrites Prepared by Auto-Combustion Technique. *Journal of Optics and Photonics Research*. https://doi.org/10.47852/bonviewJOPR62029245